

Accurate Electronic Excitation Energies In Full-Valence Active Space Via Bootstrap Embedding

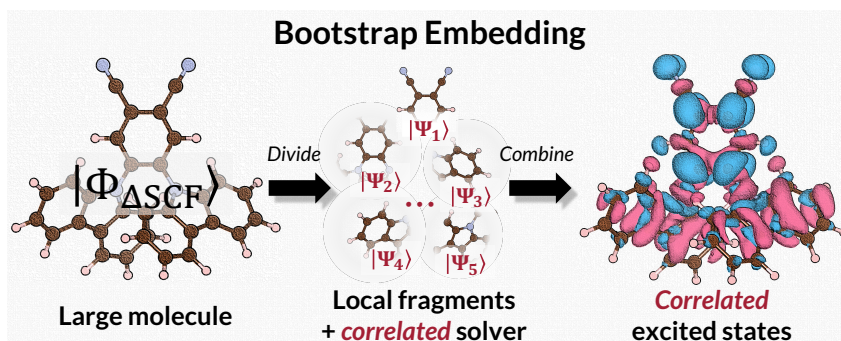
Hong-Zhou Ye, Henry K. Tran, and Troy Van Voorhis*

Department of Chemistry, Massachusetts Institute of Technology, Cambridge, MA 02139

E-mail: tvan@mit.edu

Abstract

Fragment embedding has been widely used to circumvent the high computational scaling of using accurate electron correlation methods to describe the electronic ground states of molecules and materials. However, similar applications that utilize fragment embedding to treat electronic excited states are comparably less reported in the literature. The challenge here is two-fold. First, most fragment embedding methods are most effective when the property of interest is *local*, but the change of the wave function upon excitation is *non-local* in general. Second, even for local excitations, an accurate estimate of e.g., the excitation energy, can still be challenging owing to the need for a balanced treatment of both the ground and the excited states. In this work, we show that Bootstrap Embedding (BE), a fragment embedding method developed recently by our group, is promising towards describing general electronic excitations. Numerical simulations show that the excitation energies in full-valence active space (FVAS) can be well-estimated by BE to an error of ~ 0.05 eV using relatively small fragments, for both local excitations and the excitations of some large dye molecules that exhibit strong charge-transfer characters. We hence anticipate BE to be a promising solution to accurately describing the excited states of large chemical systems.



1 Introduction

One challenge faced by using accurate electronic structure methods to solve practical problems is the high computational scaling of these methods ($O(N^p)$ where $p \geq 5$ in general) that limits the size of the systems that can be modelled computationally.^{1–10} Fragment embedding provides a promising solution to this problem by recognizing that in many cases, the interesting chemistry or physics occurs in only a local fragment of a large system,^{11–14} which can then be singled out and treated more accurately than the rest of the system to reduce the computational cost. The general idea of local fragment embedding has been realized by many authors in different contexts, each focusing on embedding a specific physical quantity, including electron densities,^{15–20} density matrices,^{21–27} molecular orbitals,^{28–32} and Green’s functions,^{33–40} to name a few.

A vast number of successful applications using these local embedding methods for both ground and excited states can be found in the literature (see refs. 17,41–45 and references therein). Most embedding calculations on excited states have been focused on local excitations, with typical applications being studying the solvatochromic shifts.^{46–55} This can be done, for instance, in the framework of wave function (WF)-in-density functional theory (DFT) embedding via subsystem DFT^{52,53,56–59} or projector-based approach,^{50,60,61} where a high-level WF method such as equation-of-motion coupled cluster^{62,63} (EOM-CC) is used to

compute the local excitations in a chosen fragment embedded in the effective potential of the environment density. The response of the environment to the fragment excitation has been shown important in many cases.^{56-58,61} Note that unlike subsystem DFT, projector-based WF-in-DFT embedding can in principle treat systems with strong fragment-environment coupling (e.g., chemical bonds)^{21,45} and hence describe non-local excitations. However, in the simple case of a delocalized $\pi \rightarrow \pi^*$ excitation, the results converge *much* more slowly than for a localized excitation,⁶⁴ so that the utility of this approach for delocalized excited states could be much lower.

In addition to local embedding, recent developments in the field have also suggested the possibility of global embedding.⁶⁵⁻⁷⁴ In a global embedding calculation, one usually starts with a low-level (e.g., mean-field) wave function of the full system and then repeatedly uses the aforementioned local embedding scheme to locally refine the wave function for a series of fragments that fully partition the system. A global quantity is then evaluated by assembling the local contributions from each fragment. Recently, we have developed Bootstrap Embedding (BE), which is a global embedding method that shows high accuracy and flexibility to compute the electronic ground states of general chemical systems.^{67,75-79} For example, we have demonstrated in previous works that BE can recover $\geq 99.5\%$ of the total correlation energy at second-order Møller-Plesset perturbation theory⁸⁰ (MP2) or coupled cluster with singles and doubles^{81,82} (CCSD) level with relatively small fragments.^{77,78}

Unlike the local embedding methods, a global embedding scheme in principle suffices to describe *any* eigenstates of the electronic Hamiltonian, including those that correspond to general, non-local excited states. As proof of concept, this has been demonstrated within the framework of Density Matrix Embedding Theory^{65,66} (DMET) using the lowest singlet excitation of a simple hydrogen trimer system.⁷³ The idea here best fits into the framework of the direct approach to excited states,⁸³⁻⁹³ where a wave function ansatz is optimized directly for a specific excited state. Perhaps the most well-known example is Δ Self-Consistent Field^{94,95} (Δ -SCF), which approximates an excited state by a single determinant and hence

parallels the ground-state Hartree-Fock⁹⁶ (HF) as well as Kohn-Sham DFT^{97,98} (KS-DFT). As a mean-field approach, Δ -SCF is known to outperform the corresponding mean-field linear response methods^{99,100} in many cases where the orbital relaxation is important for excited states.^{101–104} More importantly, recent studies have also suggested that a Δ -SCF excited state can be further improved by using traditional electron correlation methods such as MP2^{91,105} and CCSD¹⁰⁶ in a state-specific way, just like the HF ground state.

In this work, we thus combine BE and Δ -SCF to enable accurate embedding calculations for general electronic excited states. Two technical barriers have been overcome to achieve this goal. First, using BE to correct a Δ -SCF excited state in a *state-specific* manner requires one to locate the same Δ -SCF state in all fragment calculations. We achieve this by utilizing some of the recently developed algorithms that allow robust location of the desired Δ -SCF state.^{89,107} Second, previous works have suggested that BE is good at describing the valence electron correlation,^{77,78} while being less effective for the dynamic correlation in a large basis,⁷⁷ which is virtually always needed to describe an excited state. We tackle this problem by introducing the so-called full-valence active space (FVAS) that consists of orbitals of primarily valence characters extracted from a large basis. The FVAS is suitable for a BE calculation, while still being useful to describe low-lying valence excitations that are not necessarily local.

This article is organized as follows. In section 2, we review the theory of BE, discuss its extension to excited states, and present recipes for constructing the FVAS from a large basis. A local embedding scheme, local complete active space (LCAS), is also introduced to help benchmark BE’s performance on local excitations. In section 3, we present the computational details. In section 4, we numerically examine the performance of BE to predict excitation energies in FVAS. We find that BE converges quickly to the full-FVAS excitation energy with fragment size, achieving high accuracy (error ~ 0.05 eV) using relatively small fragments even for the excitations in large organic dye molecules that exhibit strong charge-transfer (CT) characters. In section 5, we conclude this work with remarks on potential future

developments.

2 Theory

A full presentation of the BE formalism can be found in the literature.⁷⁶⁻⁷⁸ Here, we briefly review the part that is relevant to this work in sections 2.1 and 2.2. Then in section 2.3, we discuss how to construct the state-specific full-valence active space that is suitable for a BE calculation. In section 2.4, we introduce a local embedding scheme, LCAS, whose performance of predicting excitation energies will be compared with BE in section 4. Throughout this work, we use “ n ” to label the electronic state.

2.1 Mean-field Schmidt decomposition

Suppose we have solved for a mean-field state (HF or Δ -SCF), $|\Phi_n\rangle$, of the system. Using the recipes that will be presented in section 2.3, a FVAS consisting of N local orbitals (LOs), $\{\chi_{\mu,n}\}_{\mu=1}^N$, can be constructed. These LOs are atom-centered and form an orthonormal set. A second-quantized Hamiltonian of the system can then be written in this state-specific LO basis

$$\hat{H}_n = \sum_{\mu\nu}^N h_{\mu\nu,n} c_{\mu,n}^\dagger c_{\nu,n} + \frac{1}{2} \sum_{\mu\nu\lambda\sigma}^N V_{\mu\nu\lambda\sigma,n} c_{\mu,n}^\dagger c_{\lambda,n}^\dagger c_{\sigma,n} c_{\nu,n}, \quad (1)$$

where \mathbf{h}_n and \mathbf{V}_n are the standard one- and two-electron (in the (11|22) order) integrals transformed to the LO basis, and $\{c_{\mu,n}^\dagger\}$ and $\{c_{\nu,n}\}$ are the creation and annihilation operators for these LOs. Since all the occupied molecular orbitals (MOs) of $|\Phi_n\rangle$ are in the span of the FVAS-LOs (section 2.3), $|\Phi_n\rangle$ is still a mean-field solution of \hat{H}_n with the same energy.

Define a fragment A in terms of the LOs from a selected set of atoms, $\{\chi_{\mu,n}\}_{\mu \in A}$, and let $N_f^A = |A|$ be the size of the fragment. The mean-field state $|\Phi_n\rangle$ can be written into a

complete active-space configuration interaction (CASCI) form⁶⁶

$$|\Phi_n\rangle = |\Phi_n^{\text{env},A}\rangle \otimes \sum_I c_{I,n}^{\text{fb},A} |\Phi_{I,n}^{\text{fb},n}\rangle, \quad (2)$$

where the CI expansion is for $2N_b^A$ electrons distributed in $(N_f^A + N_b^A)$ fragment + bath orbitals. The N_f^A fragment orbitals $\{|f_{p,n}^A\rangle\}$ are chosen to be the fragment LOs,^{78,108} while the $N_b^A (\leq N_f^A)$ entangled bath orbitals $\{|b_{p,n}^A\rangle\}$ and the disentangled environment determinant $|\Phi_n^{\text{env},A}\rangle$ can be obtained following the algorithm in appendix A. Equation (2) is called a Schmidt decomposition^{109–112} (SD) of $|\Phi_n\rangle$ on fragment A . Unlike a normal CASCI wave function, the coefficients $\{c_{I,n}^{\text{fb},A}\}$ in eq. (2) are not obtained variationally but derived from the mean-field state $|\Phi_n\rangle$ and hence encode no electron correlation. Nonetheless, we can construct an effective Hamiltonian from eq. (2) by embedding the fragment + bath subsystem in the pure environment

$$\hat{\mathcal{H}}_n^A = E_n^{\text{env},A} + \sum_{pq}^{N_f^A+N_b^A} h_{pq,n}^A a_{p,n}^{A\dagger} a_{q,n}^A + \frac{1}{2} \sum_{pqrs}^{N_f^A+N_b^A} V_{pqrs,n}^A a_{p,n}^{A\dagger} a_{r,n}^{A\dagger} a_{s,n}^A a_{q,n}^A, \quad (3)$$

where

$$E_n^{\text{env},A} = \text{Tr}(\mathbf{h}_n + \mathbf{F}_n^{\text{env},A}) \mathbf{P}_n^{\text{env},A} \quad (4)$$

$$h_{pq,n}^A = \sum_{\mu\nu}^N T_{\mu p,n}^A T_{\nu q,n}^A F_{\mu\nu,n}^{\text{env},A}, \quad (5)$$

$$V_{pqrs,n}^A = \sum_{\mu\nu\lambda\sigma}^N T_{\mu p,n}^A T_{\nu q,n}^A T_{\lambda r,n}^A T_{\sigma s,n}^A V_{\mu\nu\lambda\sigma,n}, \quad (6)$$

where $\mathbf{T}_n^A = [\mathbf{T}_n^{f,A} | \mathbf{T}_n^{b,A}]$ is the unitary matrix transforming the LOs into the fragment and the bath orbitals, $\mathbf{P}_n^{\text{env},A}$ is the environment one-particle density matrix (1PDM), and $\mathbf{F}_n^{\text{env},A}$ is the environment Fock matrix. Constructed this way, \mathcal{H}_n^A has the original mean-field state $|\Phi_n\rangle$ contained in its mean-field eigenspectrum,⁶⁶ a fact that is sometimes referred to as the exactness of HF-in-HF embedding.^{66,68} Once obtained, \mathcal{H}_n^A is solved by an electron

correlation method to calculate an accurate local wave function $|\Psi_n^A\rangle$, which allows for the computation of local observables.

An algorithm adapted from ref. 78 for efficiently evaluating the integral transform in eq. (6) is given in appendices B and C.

2.2 Bootstrap Embedding

In BE, we partition the system into a set of N_{frag} atom-based fragments. Hereafter, we use “atom” to denote an atomic group that consists of a heavy atom and all the hydrogen atoms bonded to it (e.g., a methyl group). In a BE m calculation ($m = 1, 2, \dots$), each atom carries a fragment consisting of that atom and all neighboring atoms up to the $(m-1)$ -th coordination shell. Thus, BE1 is the smallest calculation and has every atom as a fragment, BE2 adds all the nearest neighboring atoms to each fragment in BE1, and BE3 further includes the second nearest neighbors, etc. We call the atoms that are added to a fragment at BE2 and higher levels the *edge* atoms of that fragment, while the remaining one the *center* atom. Note that the union of the center atom of all fragments gives the full system.

The most important feature of these atom-centered fragments is that they *overlap* with each other (except for BE1). As a result, one atom could be an edge atom in some fragments, while being the center atom in another. In general, an atom is described at higher accuracy in the fragments where it is the center atom rather than an edge atom. This is because an edge atom lies closer to the environment, which is described at a low level of theory (i.e., mean-field).

This differential behavior of the same atom in different fragments is exploited in BE to improve the embedding. Specifically, let \mathbb{E}_A be the set of edge atoms of fragment A , and \mathbb{C}_B be the center atom of fragment B . $\mathbb{E}_A \cap \mathbb{C}_B$ then represents the atom that is better described in B than in A . To improve the quality of this edge atom of fragment A , we require the local wave function of fragment A to match the local wave function of fragment B on that atom. In this work, we choose to match the 1PDM, $P_{pq} = \langle a_q^\dagger a_p \rangle$, between fragments. This can be

achieved by a constrained optimization

$$\begin{aligned} \min_{\Psi^A} \langle \hat{\mathcal{H}}_n^A \rangle_{A,n}, \text{ s.t. } \langle a_{q,n}^{A\dagger} a_{p,n}^A \rangle_{A,n} = P_{pq,n}^B, \\ \forall p, q \in \mathbb{E}_A \cap \mathbb{C}_B, \forall B \neq A. \end{aligned} \quad (7)$$

where $\langle \cdots \rangle_{A,n} = \langle \Psi_n^A | \cdots | \Psi_n^A \rangle$, and we loop over all $B \neq A$ to enumerate all possible matching conditions for fragment A . The same analysis can be repeated for all other fragments and leads to similar density matching conditions. In addition to these fragment-specific constraints, we also impose a global constraint that fixes the sum of the electron number in the center atom of each fragment to be the total electron number of the system,

$$\sum_A^{N_{\text{frag}}} \sum_{p \in \mathbb{C}_A} \langle a_{p,n}^{A\dagger} a_{p,n}^A \rangle_{A,n} = N_e. \quad (8)$$

As shown in previous works,^{67,75} these constrained optimizations can be turned into N_{frag} coupled eigenvalue equations, one for each fragment, where the embedding Hamiltonian $\hat{\mathcal{H}}_n^A$ (eq. (3)) is dressed by (i) a fragment-specific effective potential λ_n^A that accounts for the density matching constraints (eq. (7)) and (ii) a global chemical potential μ_n that accounts for the electron number constraint (eq. (8)), i.e.,

$$\left(\hat{\mathcal{H}}_n^A + \sum_{pq \in \mathbb{E}_A} \lambda_{pq,n}^A a_{p,n}^{A\dagger} a_{q,n}^A + \mu_n \sum_{p \in \mathbb{C}_A} a_{p,n}^{A\dagger} a_{p,n}^A \right) | \Psi_n^A \rangle = \mathcal{E}_n^A | \Psi_n^A \rangle. \quad (9)$$

Equation (9) is then solved repeatedly for all fragments using some high-level method until the appropriate $\{\lambda_n^A\}$ and μ_n are found to satisfy the constraints in eqs. (7) and (8). A efficient quasi-Newton algorithm for solving this problem can be found in a previous work.⁷⁸

Once the constrained optimizations are done for all fragments, we evaluate the total

energy by summing the local contribution from each fragment center⁷⁸

$$E_n^{\text{BE}} = \sum_A \sum_{p \in C_A} \left[\sum_q \left(h_{pq,n}^A - \frac{1}{2} G_{pq,n}^{\text{env},A} \right) P_{pq,n}^A + \frac{1}{2} \sum_{qrs} V_{pqrs,n}^A \Gamma_{pqrs,n}^A \right], \quad (10)$$

where $\mathbf{G}_n^{\text{env},A}$ is the Coulomb and exchange part of the environment Fock matrix; \mathbf{P}_n^A and $\mathbf{\Gamma}_n^A$ are fragment 1PDM and 2PDM, respectively.

The formalism presented above should apply equally well to both ground ($n = 0$) and excited ($n > 0$) states, but a few comments specific to an excited state calculation using a Δ -SCF bath are needed. First, Δ -SCF often breaks the spin symmetry⁸⁴ and hence gives spin-unrestricted HF (UHF) states, because of the open-shell nature of most excited states. As shown in our previous work,⁷⁹ for BE with a UHF bath, one only needs to make two slight modifications to the protocol discussed above:

1. the density matching in eq. (7) is performed in terms of the spin-summed density matrix (i.e., $\mathbf{P}^\alpha + \mathbf{P}^\beta$), and
2. the electron number constraint in eq. (8) is made spin-dependent (i.e., two chemical potentials, μ_n^α and μ_n^β , are determined respectively to fix N_e^α and N_e^β).

Second, since we compute the BE energy by summing all fragment contributions, it is crucial that in all fragment calculations, we find the local eigenstate that best represents $|\Phi_n\rangle$; otherwise, the BE energy ceases to be state-specific. To that end, we propose the following protocol to find the local mean-field state that is most similar to $|\Phi_n\rangle$. Let \mathbf{P}_n be the 1PDM of $|\Phi_n\rangle$ in the LO basis. For each fragment A , we use the projected 1PDM,

$$\mathbf{P}_n^A = \mathbf{T}_n^{A\dagger} \mathbf{P}_n \mathbf{T}_n^A, \quad (11)$$

to initiate the SCF calculation, and then use either the maximal overlap method¹⁰⁷ (MOM) or the squared gradient minimization⁸⁹ (SGM) to help the SCF iteration stay close to the initial state. This protocol works well for all numerical examples shown below, which include

challenging cases such as the CT states in large organic dye molecules. We hence anticipate that this scheme will also work in a more general scenario.

2.3 Full-valence active space

The formalism presented in sections 2.1 and 2.2 in principle works for any choices of the local basis. Here, we choose our local basis to consist of only orbitals of valence characters, i.e., a full-valence active space (FVAS). This choice is motivated by the recently established fast convergence of BE for computing the valence correlation energy of molecules in their electronic ground states.^{77,78} An extension to treat the dynamic correlation energy with BE will be the topic of a future work.

While a FVAS can be constructed in different approaches, here, we adopt a projection-based scheme similar to the construction of the intrinsic atomic orbitals¹¹³ (IAOs). Consider a large atomic orbital (AO) basis set, $\mathbb{K} = \{\phi_\mu^v\}_{\mu=1}^N \cup \{\phi_\rho^{\text{nv}}\}_{\rho=1}^M$, which contains N valence and M non-valence (e.g., polarization) AOs. We single out the valence part and perform the following projection¹¹³

$$|\chi_{\mu,n}\rangle = [\mathcal{O}_n \tilde{\mathcal{O}}_n + (1 - \mathcal{O}_n)(1 - \tilde{\mathcal{O}}_n)]|\phi_\mu^v\rangle, \quad (12)$$

where $\mathcal{O}_n = \sum_{i \in \text{occ}} |\psi_{i,n}\rangle \langle \psi_{i,n}|$ is the projection operator onto the occupied MOs of $|\Phi_n\rangle$, and $\tilde{\mathcal{O}}_n$ is the projection operator onto the “depolarized” occupied MOs of $|\Phi_n\rangle$, defined according to ref. 113 as $|\tilde{\psi}_{i,n}\rangle = \mathcal{P}^v |\psi_{i,n}\rangle$, with \mathcal{P}^v the projection operator onto the valence AOs. Constructed this way, $\{\chi_{\mu,n}\}_{\mu=1}^N$ are valence-like orbitals that fully span the occupied MOs of $|\Phi_n\rangle$ and the $N - N_o$ virtual MOs of mainly valence character (N_o the electron occupation number), which naturally define a FVAS for the original large AO basis. For the purpose of embedding calculations, we further localize these orbitals using e.g., the Foster-Boys approach,¹¹⁴ which leads to the local basis in which we write down the Hamiltonian eq. (1).

Note that although the recipes above apply to any mean-field states, the quality of the FVAS constructed from a high-lying Δ -SCF state is expected to be low, in the sense that solving the FVAS Hamiltonian (eq. (1)) using an electron correlation method gives only a poor approximation to the full-system correlated wave function. Nonetheless, the FVAS should provide a qualitative or even semi-quantitative description to low-lying valence excited states (need not to be local), which are the type of excitations that are studied below.

2.4 Local complete active space

BE as introduced above is a global embedding method in the sense that all parts of a system are treated accurately in at least one fragment. While such a divide-and-conquer scheme is necessary for a general, non-local excited state, one may argue that a local treatment is sufficient for local excitations. Here, we introduce a local embedding scheme called local complete active space (LCAS), whose performance on local excitations will be contrasted with BE in section 4.1.

In a LCAS m calculation, one again starts with a mean-field state $|\Phi_n\rangle$ and chooses a local fragment \mathcal{A} from BE m that contains as many as possible the atoms that are responsible for the local excitation of interest. Let $\{\chi_{\mu,n}\}_{\mu=1}^{N^{\mathcal{A}}}$ be the set of LOs in \mathcal{A} . Assuming $N^{\mathcal{A}} < N_o$ (which is always true for small fragments), a singular value decomposition of the overlap matrix between the fragment LOs and the occupied MOs of $|\Phi_n\rangle$

$$S_{\mu i,n} = \langle \chi_{\mu,n} | \psi_{i,n} \rangle = \sum_p^{N^{\mathcal{A}}} \lambda_{p,n} U_{\mu p,n} V_{ip,n} \quad (13)$$

gives the $N^{\mathcal{A}}$ occupied MOs that are maximally localized in \mathcal{A} ,

$$|\bar{\psi}_{p,n}\rangle = \sum_{i \in \text{occ}} V_{ip,n} |\psi_{i,n}\rangle. \quad (14)$$

Repeating the procedure for the virtual space similarly defines the $N^{\mathcal{A}}$ virtual MOs that

are maximally overlap with \mathcal{A} . These $2N^{\mathcal{A}}$ occupied + virtual MOs naturally define a local active space for fragment \mathcal{A} , with all other $N - 2N^{\mathcal{A}}$ MOs being frozen.

One can show that these $2N^{\mathcal{A}}$ active orbitals are related to the fragment + bath orbitals coming from a SD of $|\Phi_n\rangle$ on fragment \mathcal{A} by a unitary rotation.^{78,108} Thus, an effective Hamiltonian, $\hat{\mathcal{H}}_n^{\mathcal{A}}$, that formally resembles the embedding Hamiltonian (eqs. (3) to (6)) can be constructed for the local active space and solved accurately using some electron correlation method, leading to the LCAS estimation of the total energy

$$E_n^{\text{LCAS}} = E_{\text{ECM},n}^{\mathcal{A}} + E_{\text{HF},n}^{\text{core},\mathcal{A}}, \quad (15)$$

where $E_{\text{ECM},n}^{\mathcal{A}}$ and $E_{\text{HF},n}^{\text{core},\mathcal{A}}$ are the active space energy and the energy of the frozen core determinant (cf. eq. (4)), respectively. Note that both components of the LCAS energy are state-specific, given that one finds the correct eigenstate of $\hat{\mathcal{H}}_n^{\mathcal{A}}$ that corresponds to $|\Phi_n\rangle$ (cf. the discussion at the end of section 2.2). We also note that the LCAS scheme introduced here is similar to DMET with only one fragment being treated at high level^{70,115,116} (also known as active-space DMET^{70,115} or regional embedding^{116,117}).

3 Computational details

In what follows, we assess the performance of BE to predict accurate excitation energies in FVAS using the lowest singlet excited state (S1) of a series of organic molecules shown in fig. 1. The ground state geometries optimized at the B3LYP¹¹⁸/6-31G*¹¹⁹⁻¹²³ level using the Q-Chem software package¹²⁴ are used for all molecules and can be found in the Supporting Information. All the excitations considered here are valence excitations and hence well-described by the FVAS.

These molecules can be divided into three groups. Group A consists of three singly substituted C₁₆-alkane molecules whose excitations are mainly localized to the substituents. This group is chosen to allow a direct comparison of BE, which is a global embedding

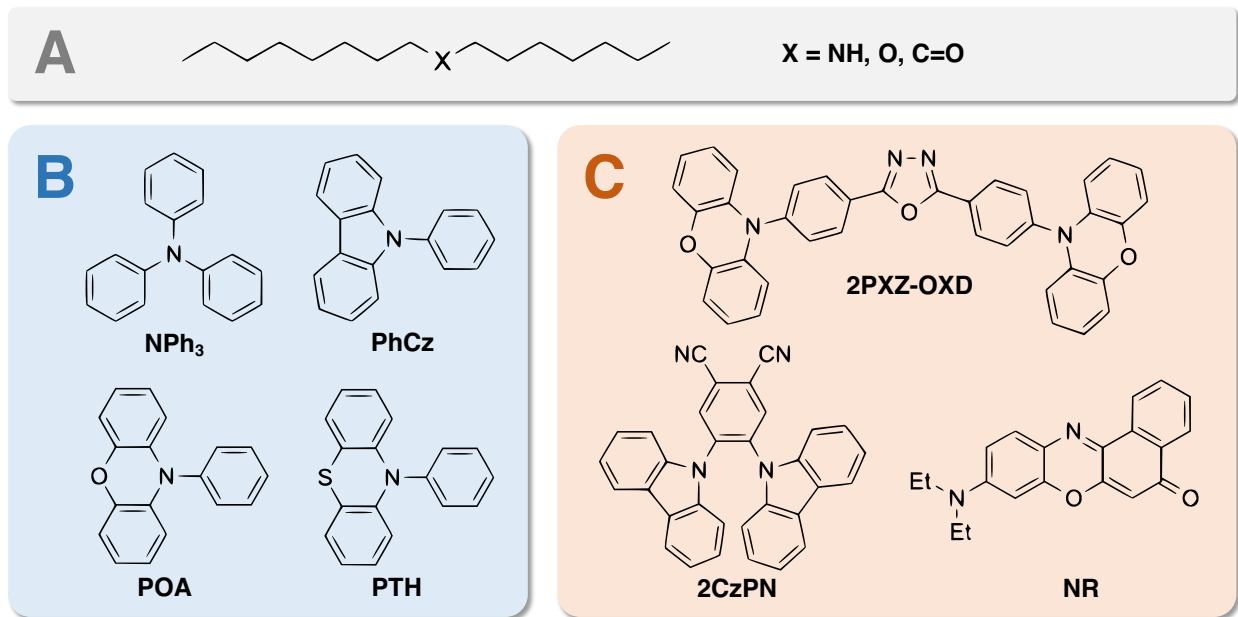


Figure 1: Lewis structure of the molecules studied in this work. Group A consists of three singly substituted C_{16} -alkanes whose excitations are mainly localized at the substituents. Group B consists of four small dye molecules that are widely used in organic photoredox catalysis. Group C consists of three larger dye molecules used in functional devices (e.g., TADF) or bioimaging.

scheme, to the local treatment, LCAS, introduced in section 2.4. Group B and C consist of small and large dye molecules, respectively, whose S1 states are not local anymore due to the conjugated π systems and hence beyond the capability of LCAS and most other local embedding methods mentioned in section 1. Some of the excitations in group C display significant CT characters, making them an excellent testbed for a global embedding method like BE.

For each molecule, we first locate the ground (HF) and the excited (Δ -SCF) state mean-field solutions using MOM or SGM (section 2.2), from which two sets of LOs that define the respective FVAS of each state are constructed according to the recipes given in section 2.3. We then perform two independent BEm (and also LCASm for group A molecules) calculations, one for each state, and use the energy difference of the two calculations as the BEm (LCASm) excitation energy. The full FVAS excitation energy is used as the benchmark, which is obtained by directly solving the FVAS Hamiltonian (eq. (1)) of both the ground

and the excited states using the same high-level method used by BE (LCAS) and then taking the energy difference.

In this work, we use the MP2 as the high-level method to solve the embedding Hamiltonians. The non-iterative nature of MP2 ensures that the correlated calculations do not swap states (unlike e.g., coupled cluster or configuration interaction), which renders it an intrinsically state-specific correction to a Δ -SCF excited state. This has been recently confirmed by our group¹⁰⁵ and others.⁹¹ The unrelaxed MP2 density matrices that ignore the SCF orbital relaxation as implemented in the PySCF software package¹²⁵ are used for the BE density matching (eqs. (7) and (8)) as well as the energy evaluation (eq. (10)). This choice has been shown in previous works to give better BE energies compared to the relaxed densities.^{77,78}

In all BE calculations, the constraint on the electron number (eq. (8)) is fully imposed, while the constraints on the 1PDM of overlapping fragments (eq. (7)) are imposed both fully and partially to investigate their effects on accuracy. Specifically, we distinguish two types of density matching constraints: one applied to an *intra*-atomic block of the 1PDM, the other applied to an *inter*-atomic block of the 1PDM. We use the notations $BE_m(0)$ for a one-shot calculation that does not impose any density matching constraints, $BE_m(1)$ for a calculation that imposes only the intra-atomic constraints, and $BE_m(2)$ for a calculation that further imposes the inter-atomic constraints. Note that the distinction between $BE_m(1)$ and $BE_m(2)$ only affects BE3 and higher level calculations where fragments can overlap at two or more atoms.

We implemented BE and LCAS as described above in a home-made code using PySCF¹²⁵ and Libint2¹²⁶ as backends for basic electronic structure modules. Core MOs are frozen for both ground and excited state calculations of all molecules, which has been checked for selected molecules to introduce negligible errors (< 0.01 eV) to the calculated excitation energy. Density fitting^{127–130} and integral screening^{131–134} are used to accelerate the integral transformation in eq. (6) using the algorithm presented in appendix B. The bath disen-

tanglement problem and its solution are discussed in appendix C; we use a cutoff of 10^{-6} for selecting the entangled bath orbitals (see appendix C for details). The cc-pVDZ^{135,136} (cc-pVDZ-RI¹³⁷) basis set is used as the working (auxiliary) basis for the BE calculations of group A molecules, while def2-SVP¹³⁸ (def2-SVP-C¹³⁹) is used for all other molecules. A BE calculation is deemed converged when both the root mean squared error of all the constraints and the energy change from previous iteration drop below 10^{-6} (both in atomic unit).

4 Results and discussion

4.1 Local excitations

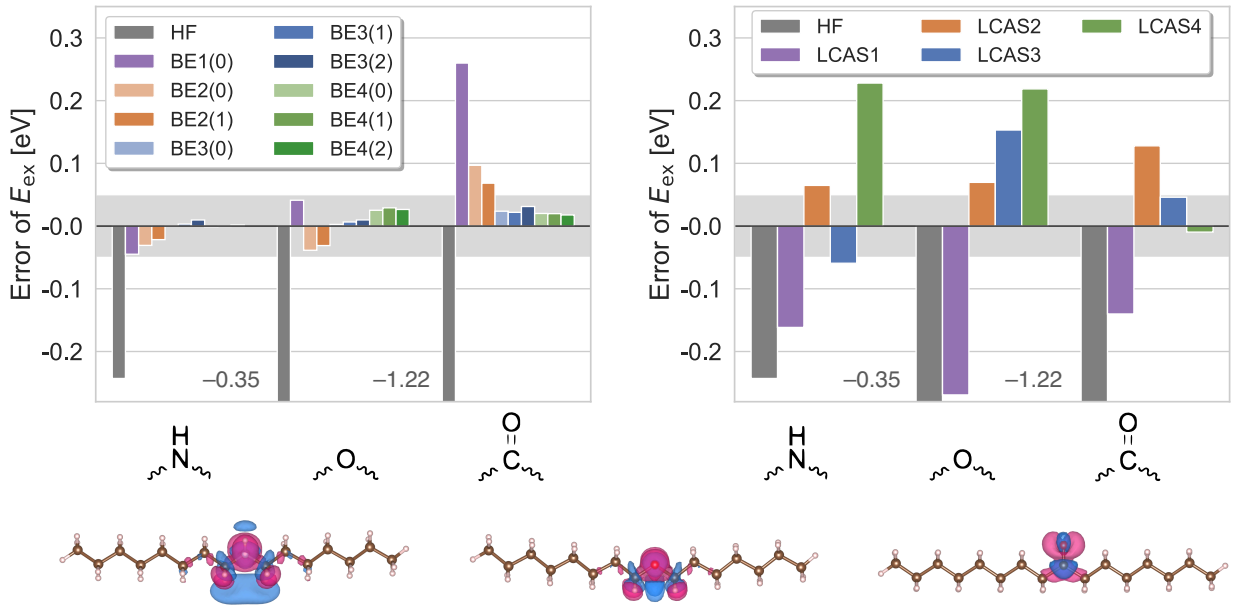


Figure 2: Upper panel: errors of the S1 excitation energies of three singly substituted alkanes (fig. 1, group A) calculated by BE (left) and LCAS (right) with increasing fragment size. For errors exceeding the limit of the y -axis, the values are listed aside. The grey shaded area indicates an absolute error below 0.05 eV. Lower panel: density difference plots (hole is colored in red) at the mean-field level (from left to right: amine, ether, and ketone), which indicate that all three excitations are local to the substituents.

We first consider the three singly substituted alkanes in fig. 1A. As mentioned above,

these excitations are expected to be localized to the substituents. This is confirmed by the density difference plots between the HF and the Δ -SCF states shown in the lower panel of fig. 2 (see fig. S1 for a zoomed-in view). The errors of the excitation energies computed by BE and LCAS using different-sized fragments are plotted in the upper panel of fig. 2.

Overall, the excitation energy predicted by BE shows fast convergence with fragment size to the full-FVAS number: an error of < 0.05 eV (grey shaded area in fig. 2) is already achieved at the BE2 level for the amine and the ether, and at the BE3 level for the ketone. Further increasing the fragment size either continues to improve the results (for the ketone) or maintains the (already high) accuracy from the small-fragment calculations (for the amine and the ether). The effect of imposing the density matching constraints (eq. (7)), which can be seen from comparing $BE_m(0)$ to $BE_m(1)$ and $BE_m(2)$, is significant only for small fragments for these simple systems.

The good performance of BE contrasts sharply with the scattered results of LCAS. For the ketone, LCAS shows similarly good convergence compared to BE. For the other two molecules, however, a large, negative error of LCAS1 is gradually turned into a large, positive error by increasing the fragment size to LCAS4, indicating a slow and non-monotonic convergence with fragment size. These results are perhaps unexpected given that all three excitations considered here are simple, local excitations.

Generally speaking, an accurate energy difference from a local treatment must rely to some extent on the error cancellation between the two independent calculations. The results in fig. 2 hence suggest that BE gives a more balanced description between the ground and the excited states of a molecule compared to LCAS. This can be seen more clearly from the total correlation energies listed in tables S1 and S2 in the Supporting Information. The BE correlation energy quickly converges to an error of $0.03 \sim 0.05$ eV at the BE3 level for both the ground and the excited states of all three molecules, while for LCAS, an error of ~ 5 eV remains even at the LCAS4 level.

We note that similar systems have been studied recently by Wen and co-workers⁶¹ using

projection-based WF-in-DFT embedding. They reported a similar error of $0.1 \sim 0.2$ eV when using fragments of size comparable to LCAS1 ~ 4 . However, a relatively monotonic convergence with fragment size was seen in their work. We thus conclude that even for simple, local excitations, one needs to be careful to achieve a balanced treatment of both states and BE, as a global embedding scheme, provides a promising solution.

4.2 Non-local excitations

In this section, we move on to study some non-local excitations that go beyond the capability of a local embedding treatment such as LCAS. We first consider the four small dye molecules shown in fig. 1, group B. These molecules share a similar structure with a central heteroatom surrounded by a few small aromatic rings, making the S1 state a weak CT state from the center to the periphery (fig. 3, right panel). The errors of the BE estimated excitation energies are plotted in the left panel of fig. 3.

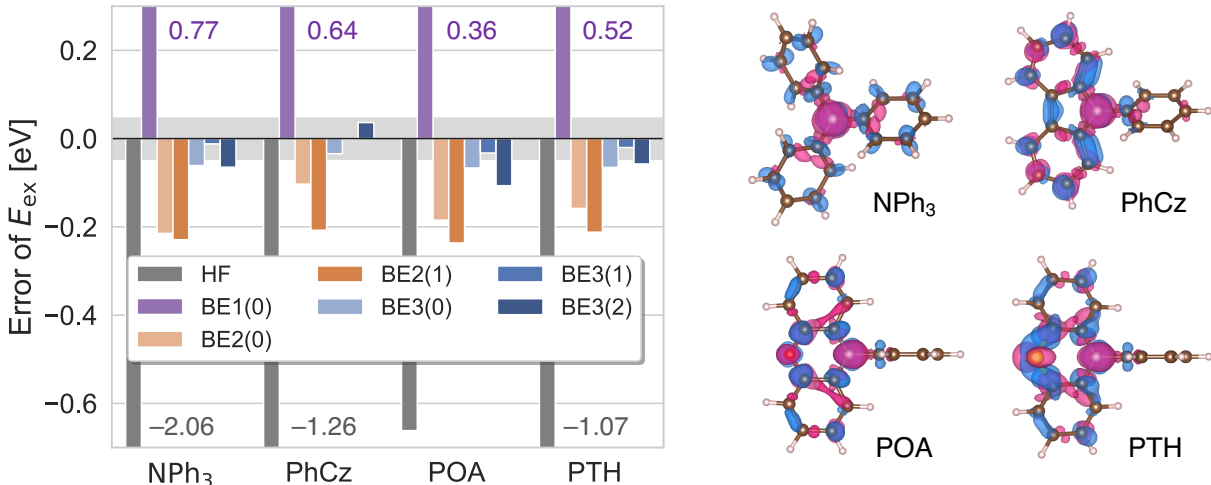


Figure 3: Left panel: errors of the S1 excitation energies of four small dye molecules (fig. 1, group B) predicted by BE with increasing fragment size. For errors exceeding the limit of the y -axis, the values are listed aside. The grey shaded area indicates an absolute error below 0.05 eV. Right panel: density difference plots (hole is colored in red) at the mean-field level, which indicate that all four excitations are non-local and display a weak CT character from the central heteroatom to the surrounding aromatic rings.

The overall performance of BE is slightly worse here than in the previous examples of local

excitations. BE2 reduces the large error of BE1 to $0.1 \sim 0.2$ eV, and BE3 further reduces this number to ~ 0.05 eV. The effect of density matching is more significant here compared to the previous examples. Specifically, BE2(1) tends to slightly increase the error of BE2(0), while BE3(1) gives better performance than both BE3(0) and BE3(2). An examination of the BE total correlation energies corresponding to these excitations (table S3) suggests that the scattered effect of density matching is not due to it being ineffective. On the contrary, imposing more constraints monotonically decreases the errors of the BE correlation energy for both the ground and the excited states in virtually all cases. Thus, it is the (small) differential improvements brought by the density matching to the two states that are responsible for the anti-corrections observed above. This is at least partially due to the bath disentanglement issue that occurs to a different extent for the two states (fig. S2).

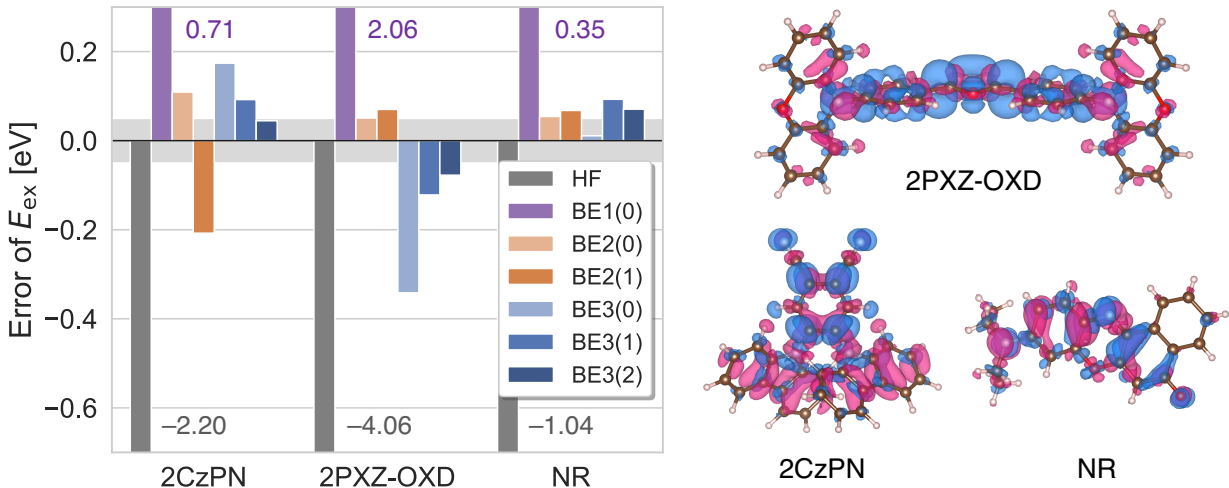


Figure 4: Same plots as those in fig. 3 for three large dye molecules (fig. 1, group C). The density difference plots (hole is colored in red) shown on the right indicate that the excitations are strongly delocalized across the large conjugated π systems and exhibit significant CT characters.

As a final test, we examine the performance of BE using three large dye molecules (fig. 1, group C). Two of them, namely 2CzPN and 2PXZ-OXD, have been used as candidate molecules for thermally activated delayed fluorescence^{140–142} (TADF) due to the strong CT characters of the S1 state, while the third one, Nile red (NR), is a commercial dye that has been used in bioimaging.¹⁴³ The characters of these excitations can be seen from the density

difference plots shown in the right panel of fig. 4. The errors of the BE excitation energies are plotted in the left panel of fig. 4.

The overall trend of convergence with fragment size is similar to what has been observed in fig. 3. The large error of BE1 is reduced to slightly above the 0.05 eV threshold at the BE2 level, and BE3 either maintains the (already high) accuracy (for 2PXZ-OXD and NR) or brings further improvement (for 2CzPN). The effect of density matching is more significant here at the BE3 level compared to the previous examples, especially for the two TADF molecules where significant charge redistribution is induced by the strong CT excitations. However, compared to the small dye molecules, the larger ones have more fragments exhibiting different extent of bath disentanglement in the ground and the excited states (fig S2). Thus, a small but non-negligible error cancellation contributes to the good performance observed in fig. 4.

The convergence of the excitation energies with both the fragment size and the level of density matching observed here is consistent with the convergence of the total correlation energy, as can be seen from table S4. However, we note that in these cases the BE total correlation energy is not as accurate as in previous examples, with BE3 having a typical error of $\sim 2\%$ or ~ 1 eV (table S4). Interestingly, the number of disentangled bath orbitals does not show a significant difference between the two groups of dye molecules (table S5), which suggests that a better metric for measuring the bath disentanglement is needed to resolve the observed different performance of BE, which we plan to explore in future work. Nonetheless, the fact that BE can deliver accurate excitation energies of ~ 0.05 eV error even for these strongly non-local excitations is encouraging for future developments.

5 Conclusion

In conclusion, we have extended Bootstrap Embedding, a previously developed ground state quantum embedding method, to calculating the excitation energies in full-valence active

space for molecules. As a global embedding method, BE achieves high accuracy in the calculated excitation energies by treating both the ground and the excited states to equally high accuracy. This contrasts with the traditional local embedding schemes that rely on the large error cancellation of two inaccurate simulations. Numerical results confirmed BE’s superiority over a local embedding scheme, LCAS, even for simple, local excitations. More importantly, for general, delocalized excitations beyond the capability of a local treatment, BE continues to deliver highly accurate excitation energies using relatively small fragments that span up to two chemical bonds (i.e., BE3).

In the future, the computational protocol introduced here could be extended in the following directions. First, since the goal of BE is to precisely reproduce whatever the full calculation is, the accuracy of the full calculation determines how useful it is in practice. In this regard, the spin-unrestricted MP2 (UMP2) method used here is suboptimal for known issues such as spin-contamination.^{144–146} Fortunately, it has been shown that most of the problems of the bare UMP2 can be largely mitigated by adopting another reference state (e.g., the spin-restricted open-shell MP2¹⁰⁵), using KS-DFT orbitals and scaled energy,¹⁴⁷ or incorporating scaled MP3 corrections.^{148–152} In addition, recent works have also suggested the possibility of combining coupled cluster with Δ -SCF for excited states.¹⁰⁶ Thus, a straightforward next-step is to adapt BE for these local solvers to enable more accurate BE calculations for excited states.

Second, while FVAS may be a good approximation to many low-lying valence excitations, it could fail quantitatively and even qualitatively in other cases. Thus, it is desirable to have BE be able to compute excited states in a large basis with polarization and even diffuse functions. As mentioned above and detailed in a previous work,⁷⁷ disentanglement of the mean-field bath is the main challenge here. However, recent developments from our research group have suggested that this issue may be alleviated to a large extent by an appropriate choice of the local basis. Such a development will benefit BE in both the ground and the excited state calculations, which will be investigated in a future work.

With these potential future developments, we anticipate BE to be a promising embedding method that can describe general electronic excitations in a large chemical system.

Supporting Information

(i) A zoomed-in view of the density difference plots in fig. 2. (ii) Visualization of BE3-level fragments that exhibit different bath disentanglement in the ground and the excited states. (iii) Total MP2 correlation energy and energy error obtained from BE (for all three groups) and LCAS (for group A only). (iv) Number of entangled bath orbitals averaged over all BE3-level fragments for the dye molecules from group B and group C.

Acknowledgement

HY thanks Zhi-Hao Cui for discussion on how to obtain the intrinsic atomic orbitals. This work was funded by a grant from the NSF (Grant No. CHE-1900358).

A Schmidt decomposition of a mean-field state

Hereafter, we drop the state label “ n ” for simplicity, but the discussion below applies to any mean-field states.

Let $|\Phi\rangle$ be a mean-field state and \mathbf{P} its 1PDM in the LO basis. Let the first N_A LOs comprise fragment A . \mathbf{P} has the following block structure

$$\mathbf{P} = \begin{bmatrix} \mathbf{P}_{AA} & \mathbf{P}_{A\bar{A}} \\ \mathbf{P}_{\bar{A}A} & \mathbf{P}_{\bar{A}\bar{A}} \end{bmatrix} \quad (16)$$

where we use \bar{A} to denote the LOs outside fragment A . Diagonalizing $\mathbf{P}_{\bar{A}\bar{A}}$ gives the following

eigenvectors and eigenvalues

$$\mathbf{U}_{\bar{A}} = \begin{bmatrix} \mathbf{U}_b^A & \mathbf{U}_{\text{eo}}^A & \mathbf{U}_{\text{ev}}^A \end{bmatrix}, \quad \mathbf{\Lambda}_{\bar{A}} = \begin{bmatrix} \mathbf{\Lambda}^A & & \\ & \mathbf{1}_{N_o-N_A} & \\ & & \mathbf{0}_{N_v-N_A} \end{bmatrix} \quad (17)$$

where $\mathbf{\Lambda}^A = \text{diag}\{\lambda_1^A, \dots, \lambda_{N_A}^A\}$ collects eigenvalues that lie between 0 and 1, \mathbf{U}_b^A defines the entangled bath orbitals (BOs) $\{|b_p^A\rangle\}_{p=1}^{N_A}$, and \mathbf{U}_{eo}^A and \mathbf{U}_{ev}^A respectively define the occupied and virtual orbitals of the environment determinant $|\Phi^{\text{env},A}\rangle$. With our choice of fragment LOs as the fragment orbitals (FOs) (section 2.1), the Schmidt orbital (SO) coefficient matrix \mathbf{T}^A is simply

$$\mathbf{T}^A = \begin{bmatrix} \mathbf{1}_{N_A} & \mathbf{0} \\ \mathbf{0} & \mathbf{U}_b^A \end{bmatrix}. \quad (18)$$

Note that unlike the algorithm presented in previous works,^{66,108,153} the algorithm above does not involve normalizing the BOs using λ , which could cause numerical issues when $\lambda \sim 0$. Instead, one can obtain the BOs directly from the eigenvectors $\{\mathbf{u}_p\}$ of $\mathbf{P}_{\bar{A}\bar{A}}$ by sorting them by their eigenvalues in ascending order and choosing $\mathbf{u}_{N_v-N_A+1}, \dots, \mathbf{u}_{N_v}$.

B Algorithm for BE ERI transform

For fragments that overlap with each other, calculating the fragment ERIs by directly applying eq. (6) to each fragment is inefficient since the ERIs of the overlapping regions of different fragments are related and need to be evaluated only once. Here, we review an efficient algorithm developed in a previous work⁷⁸ that avoids any redundant computation. In appendix C, we discuss an issue of this algorithm arising from the bath disentanglement problem and a potential solution.

Let $A = \{a_1, \dots, a_L\}$ be an L -atom fragment (lowercase a 's label atoms hereafter), and

\mathbf{T}^A and $\{\mathbf{T}^{a_i}\}$ be the corresponding SOs. Define

$$\mathbf{W}^A = (\tilde{\mathbf{T}}^{A\dagger}\tilde{\mathbf{T}}^A)^{-1}\tilde{\mathbf{T}}^{A\dagger}\mathbf{T}^A, \quad (19)$$

which relates the atom-SOs $\tilde{\mathbf{T}}^A = [\mathbf{T}^{a_1} | \dots | \mathbf{T}^{a_L}]$ to the fragment-SOs,

$$\mathbf{T}^A = \tilde{\mathbf{T}}^A \mathbf{W}^A. \quad (20)$$

Now let $\mathbb{Q}_A = \{(a_i, a_j, a_k, a_l) | a_i, a_j, a_k, a_l \in A\}$ be the set of atom-quartets that are connected in A . With eq. (20), we can compute the fragment ERIs \mathbf{V}^A by first calculating the atom-quartet ERIs

$$\mathbf{V}^{a_i a_j a_k a_l} = \mathbf{T}^{a_i\dagger} \mathbf{T}^{a_j\dagger} \mathbf{V} \mathbf{T}^{a_k} \mathbf{T}^{a_l} \quad (21)$$

for all $(a_i, a_j, a_k, a_l) \in \mathbb{Q}_A$, and then transforming them using \mathbf{W}^A

$$\mathbf{V}^A = \mathbf{W}^{A\dagger} \mathbf{W}^{A\dagger} \tilde{\mathbf{V}}^A \mathbf{W}^A \mathbf{W}^A, \quad (22)$$

where $\tilde{\mathbf{V}}^A$ has $\mathbf{V}^{a_i a_j a_k a_l}$ as its (a_i, a_j, a_k, a_l) -block for all $(a_i, a_j, a_k, a_l) \in \mathbb{Q}_A$. Note that eq. (21) scales as $O(N_a N^4)$ and eq. (22) scales as $O(N_A^5)$, with N_a the typical number of LOs of an atom. Since $N_A \ll N$, the computation of the atom-quartet ERIs is the slow step.

Now for a set of overlapping fragments $\{A\}$, we first compute the atom-quartet ERIs $\mathbf{V}^{a_i, a_j, a_k, a_l}$ for all $(a_i, a_j, a_k, a_l) \in \bigcup_A \mathbb{Q}_A$ using eq. (21) and then apply eq. (22) to obtain the corresponding fragment ERIs $\{\mathbf{V}^A\}$. This two-step algorithm is efficient for overlapping fragments since it performs the slow transform eq. (21) only for the unique atom-quartets given by $\bigcup_A \mathbb{Q}_A$.

C Handling bath disentanglement

In eq. (19), we assume that $\tilde{\mathbf{T}}^A$ is full column rank so that $\tilde{\mathbf{T}}^{A\dagger}\tilde{\mathbf{T}}^A$ is invertible. However, when some BOs are disentangled from the fragment, with the corresponding λ in eq. (17) being close to 0 or 1, linear dependency is found in the column space of $\tilde{\mathbf{T}}^A$. When this occurs, we first turn $\tilde{\mathbf{T}}^A$ into a similar block structure as \mathbf{T}^A ,

$$\tilde{\mathbf{T}}^A \mathbf{R}_1^A \mathbf{R}_2^A = \begin{bmatrix} \mathbf{1}_{N_A} & \mathbf{0} \\ \mathbf{0} & \tilde{\mathbf{U}}_b^A \end{bmatrix}, \quad (23)$$

where \mathbf{R}_1^A permutes all the fragment orbitals to the left and \mathbf{R}_2^A eliminates the upper-right block of the $\tilde{\mathbf{T}}^A \mathbf{R}_1^A$. Equation (23) condenses all the linear dependency of $\tilde{\mathbf{T}}^A$ in the N_A atom-BOs, $\tilde{\mathbf{U}}_b^A$. Canonical orthonormalization gives the n_A ($< N_A$) linearly independent atom-BOs,

$$\hat{\mathbf{U}}_b^A = \tilde{\mathbf{U}}_b^A \hat{\mathbf{X}}_b^A (\hat{\mathbf{\Sigma}}_b^A)^{-1/2}, \quad (24)$$

where $\hat{\mathbf{X}}_b^A$ collects the non-singular eigenvectors of $\tilde{\mathbf{U}}_b^{A\dagger}\tilde{\mathbf{U}}_b^A$ (identified by eigenvalues $\hat{\mathbf{\Sigma}}_b^A$ greater than some threshold τ). A subsequent singular value decomposition of the overlap matrix between the atom- and the fragment-BOs,

$$\hat{\mathbf{U}}_b^{A\dagger} \mathbf{U}_b^A = \mathbf{Y}_b^A \begin{bmatrix} \mathbf{\Delta}_b^A & \mathbf{0} \end{bmatrix} \begin{bmatrix} \mathbf{Z}_{b,1}^A & \mathbf{Z}_{b,2}^A \end{bmatrix}^\dagger, \quad (25)$$

splits the fragment-BOs \mathbf{U}_b^A into an entangled and a disentangled part,

$$\mathbf{U}_b^A \begin{bmatrix} \mathbf{Z}_{b,1}^A & \mathbf{Z}_{b,2}^A \end{bmatrix} = \begin{bmatrix} \mathbf{U}_{b,\text{ent}}^A & \mathbf{U}_{b,\text{disent}}^A \end{bmatrix}, \quad (26)$$

where only the n_A entangled fragment-BOs can be computed from the atom-BOs,

$$\mathbf{U}_{b,\text{ent}}^A = \hat{\mathbf{U}}_b^A \mathbf{Y}_b^A (\mathbf{\Delta}_b^A)^{-1}. \quad (27)$$

Now let

$$\mathbf{W}^A = \mathbf{R}_1^A \mathbf{R}_2^A \begin{bmatrix} \mathbf{1}_{N_A} & \mathbf{0} \\ \mathbf{0} & \hat{\mathbf{X}}_b^A (\hat{\Sigma}_b^A)^{-1/2} \mathbf{Y}_b^A (\Delta_b^A)^{-1} \end{bmatrix}, \quad (28)$$

and use it in the BE ERI transform algorithm (appendix B). The thus computed \mathbf{V}^A is non-zero only when all four indices correspond to either the FOs or the entangled BOs. In other words, the disentangled BOs become non-interacting at the two-body level (they still interact at the one-body level) and hence formulate a non-interacting bath.¹¹⁵ We find that this double-bath (an interacting bath via $\mathbf{U}_{b,\text{ent}}$ and a non-interacting bath via $\mathbf{U}_{b,\text{disent}}$) scheme works well for all examples studied in this work.

References

- (1) Fortenberry, R. C. The ArNH^{2+} noble gas molecule: Stability, vibrational frequencies, and spectroscopic constants. *J. Mol. Spectrosc.* **2019**, *357*, 4 – 8.
- (2) Theis, M. L.; Candian, A.; Tielens, A. G. G. M.; Lee, T. J.; Fortenberry, R. C. Electronically Excited States of Anisotropically Extended Singly-Deprotonated PAH Anions. *J. Phys. Chem. A* **2015**, *119*, 13048–13054.
- (3) Fortenberry, R. C.; Novak, C. M.; Layfield, J. P.; Matito, E.; Lee, T. J. Overcoming the Failure of Correlation for Out-of-Plane Motions in a Simple Aromatic: Rovibrational Quantum Chemical Analysis of $c\text{-C}_3\text{H}_2$. *J. Chem. Theory Comput.* **2018**, *14*, 2155–2164.
- (4) Mabrouk, N.; Berriche, H. Theoretical study of the NaLi molecule: potential energy curves, spectroscopic constants, dipole moments and radiative lifetimes. *J. Phys. B: At. Mol. Opt. Phys* **2008**, *41*, 155101.
- (5) Chien, A. D.; Holmes, A. A.; Otten, M.; Umrigar, C. J.; Sharma, S.; Zimmerman, P. M.

- Excited States of Methylene, Polyenes, and Ozone from Heat-Bath Configuration Interaction. **2018**, *122*, 2714–2722.
- (6) Stemmler, C.; Paulus, B.; Legeza, O. Analysis of electron-correlation effects in strongly correlated systems (N_2 and N_2^+) by applying the density-matrix renormalization-group method and quantum information theory. *Phys. Rev. A* **2018**, *97*, 022505.
- (7) Hachmann, J.; Dorando, J. J.; Avilés, M.; Chan, G. K.-L. The radical character of the acenes: A density matrix renormalization group study. *J. Chem. Phys.* **2007**, *127*, 134309.
- (8) Taffet, E. J.; Scholes, G. D. The A_g^+ state falls below ${}^3A_g^-$ at carotenoid-relevant conjugation lengths. *Chem. Phys.* **2017**,
- (9) Pantazis, D. A. Meeting the Challenge of Magnetic Coupling in a Triply-Bridged Chromium Dimer: Complementary Broken-Symmetry Density Functional Theory and Multireference Density Matrix Renormalization Group Perspectives. *J. Chem. Theory Comput.* **2019**, *15*, 938–948.
- (10) Hajgató, B.; Szieberth, D.; Geerlings, P.; De Proft, F.; Deleuze, M. S. A benchmark theoretical study of the electronic ground state and of the singlet-triplet split of benzene and linear acenes. *J. Chem. Phys.* **2009**, *131*, 224321.
- (11) Eisenmesser, E. Z.; Bosco, D. A.; Akke, M.; Kern, D. Enzyme Dynamics During Catalysis. *Science* **2002**, *295*, 1520–1523.
- (12) Benkovic, S. J.; Hammes-Schiffer, S. A Perspective on Enzyme Catalysis. *Science* **2003**, *301*, 1196–1202.
- (13) Liu, J.; Wang, S.; Huang, T.; Manchanda, P.; Abou-Hamad, E.; Nunes, S. P. Smart covalent organic networks (CONs) with “on-off-on” light-switchable pores for molecular separation. *Sci. Adv.* **2020**, *6*.

- (14) Prawer, S.; Greentree, A. D. Diamond for Quantum Computing. *Science* **2008**, *320*, 1601–1602.
- (15) Senatore, G.; Subbaswamy, K. R. Density dependence of the dielectric constant of rare-gas crystals. *Phys. Rev. B* **1986**, *34*, 5754–5757.
- (16) Johnson, M. D.; Subbaswamy, K. R.; Senatore, G. Hyperpolarizabilities of alkali halide crystals using the local-density approximation. *Phys. Rev. B* **1987**, *36*, 9202–9211.
- (17) Jacob, C. R.; Neugebauer, J. Subsystem density-functional theory. *Wiley Interdiscip. Rev. Comput. Mol. Sci* **2014**, *4*, 325–362.
- (18) Huang, C.; Carter, E. A. Potential-functional embedding theory for molecules and materials. *J. Chem. Phys.* **2011**, *135*, 194104.
- (19) Huang, C.; Pavone, M.; Carter, E. A. Quantum mechanical embedding theory based on a unique embedding potential. *J. Chem. Phys.* **2011**, *134*, 154110.
- (20) Yu, K.; Libisch, F.; Carter, E. A. Implementation of density functional embedding theory within the projector-augmented-wave method and applications to semiconductor defect states. *J. Chem. Phys.* **2015**, *143*, 102806.
- (21) Manby, F. R.; Stella, M.; Goodpaster, J. D.; Miller, T. F. A Simple, Exact Density-Functional-Theory Embedding Scheme. *J. Chem. Theory Comput.* **2012**, *8*, 2564–2568.
- (22) Goodpaster, J. D.; Barnes, T. A.; Manby, F. R.; Miller, T. F. Accurate and systematically improvable density functional theory embedding for correlated wavefunctions. *J. Chem. Phys.* **2014**, *140*, 18A507.
- (23) Fornace, M. E.; Lee, J.; Miyamoto, K.; Manby, F. R.; Miller, T. F. Embedded Mean-Field Theory. *J. Chem. Theory Comput.* **2015**, *11*, 568–580.

- (24) Chulhai, D. V.; Goodpaster, J. D. Projection-Based Correlated Wave Function in Density Functional Theory Embedding for Periodic Systems. *J. Chem. Theory Comput.* **2018**, *14*, 1928–1942.
- (25) Yu, K.; Carter, E. A. Extending density functional embedding theory for covalently bonded systems. *Proc. Natl. Acad. Sci.* **2017**, *114*, E10861–E10870.
- (26) Huang, C. Embedded Cluster Density Approximation for Exchange-Correlation Energy: A Natural Extension of the Local Density Approximation. *J. Chem. Theory Comput.* **2018**, *14*, 6211–6225.
- (27) Zhang, X.; Carter, E. A. Subspace Density Matrix Functional Embedding Theory: Theory, Implementation, and Applications to Molecular Systems. *J. Chem. Theory Comput.* **2019**, *15*, 949–960.
- (28) Kitaura, K.; Ikeo, E.; Asada, T.; Nakano, T.; Uebayasi, M. Fragment molecular orbital method: an approximate computational method for large molecules. *Chem. Phys. Lett.* **1999**, *313*, 701 – 706.
- (29) Fedorov, D. G.; Kitaura, K. The importance of three-body terms in the fragment molecular orbital method. *J. Chem. Phys.* **2004**, *120*, 6832–6840.
- (30) Khaliullin, R. Z.; Head-Gordon, M.; Bell, A. T. An efficient self-consistent field method for large systems of weakly interacting components. *J. Chem. Phys.* **2006**, *124*, 204105.
- (31) Fedorov, D. G.; Kitaura, K. Extending the Power of Quantum Chemistry to Large Systems with the Fragment Molecular Orbital Method. *J. Phys. Chem. A* **2007**, *111*, 6904–6914.
- (32) Macetti, G.; Wieduwilt, E. K.; Assfeld, X.; Genoni, A. Localized Molecular Orbital-Based Embedding Scheme for Correlated Methods. *J. Chem. Theory Comput.* **2020**, *16*, 3578–3596.

- (33) Metzner, W.; Vollhardt, D. Correlated Lattice Fermions in $d = \infty$ Dimensions. *Phys. Rev. Lett.* **1989**, *62*, 324–327.
- (34) Georges, A.; Krauth, W. Numerical solution of the $d = \infty$ Hubbard model: Evidence for a Mott transition. *Phys. Rev. Lett.* **1992**, *69*, 1240–1243.
- (35) Georges, A.; Kotliar, G.; Krauth, W.; Rozenberg, M. J. Dynamical mean-field theory of strongly correlated fermion systems and the limit of infinite dimensions. *Rev. Mod. Phys.* **1996**, *68*, 13–125.
- (36) Kotliar, G.; Savrasov, S. Y.; Haule, K.; Oudovenko, V. S.; Parcollet, O.; Marianetti, C. A. Electronic structure calculations with dynamical mean-field theory. *Rev. Mod. Phys.* **2006**, *78*, 865–951.
- (37) Maier, T.; Jarrell, M.; Pruschke, T.; Hettler, M. H. Quantum cluster theories. *Rev. Mod. Phys.* **2005**, *77*, 1027–1080.
- (38) Turkowski, V.; Kabir, A.; Nayyar, N.; Rahman, T. S. Dynamical mean-field theory for molecules and nanostructures. *J. Chem. Phys.* **2012**, *136*, 114108.
- (39) Zhu, T.; Cui, Z.-H.; Chan, G. K.-L. Efficient Formulation of *Ab Initio* Quantum Embedding in Periodic Systems: Dynamical Mean-Field Theory. *J. Chem. Theory Comput.* **2020**, *16*, 141–153.
- (40) Zhu, T.; Chan, G. K.-L. *Ab Initio* Full Cell GW+DMFT for Correlated Materials. 2020.
- (41) Vreven, T.; Morokuma, K. In *Hybrid Methods: ONIOM(QM:MM) and QM/MM*; Spellmeyer, D. C., Ed.; Ann. Rep. Comput. Chem.; Elsevier, 2006; Vol. 2; pp 35 – 51.
- (42) Lin, H.; Truhlar, D. G. QM/MM: what have we learned, where are we, and where do we go from here? *Theor. Chem. Acc.* **2007**, *117*, 185.

- (43) Gordon, M. S.; Fedorov, D. G.; Pruitt, S. R.; Slipchenko, L. V. Fragmentation Methods: A Route to Accurate Calculations on Large Systems. *Chem. Rev.* **2012**, *112*, 632–672.
- (44) Yu, K.; Krauter, C. M.; Dieterich, J. M.; Carter, E. A. *Fragmentation*; John Wiley & Sons, Ltd, 2017; Chapter 2, pp 81–117.
- (45) Lee, S. J. R.; Welborn, M.; Manby, F. R.; Miller, T. F. Projection-Based Wavefunction-in-DFT Embedding. *Acc. Chem. Res.* **2019**, *52*, 1359–1368.
- (46) Krauss, M. Effective fragment potentials and spectroscopy at enzyme active sites. *Comput. Chem.* **1995**, *19*, 33 – 38.
- (47) Yoo, S.; Zahariev, F.; Sok, S.; Gordon, M. S. Solvent effects on optical properties of molecules: A combined time-dependent density functional theory/effective fragment potential approach. *J. Chem. Phys.* **2008**, *129*, 144112.
- (48) Kina, D.; Arora, P.; Nakayama, A.; Noro, T.; Gordon, M. S.; Taketsugu, T. *Ab initio* QM/MM excited-state molecular dynamics study of coumarin 151 in water solution. **2009**, *109*, 2308–2318.
- (49) Arora, P.; Slipchenko, L. V.; Webb, S. P.; DeFusco, A.; Gordon, M. S. Solvent-Induced Frequency Shifts: Configuration Interaction Singles Combined with the Effective Fragment Potential Method. **2010**, *114*, 6742–6750.
- (50) Bennie, S. J.; Curchod, B. F. E.; Manby, F. R.; Glowacki, D. R. Pushing the Limits of EOM-CCSD with Projector-Based Embedding for Excitation Energies. *J. Phys. Chem. Lett.* **2017**, *8*, 5559–5565.
- (51) Hedegård, E. D.; Reiher, M. Polarizable Embedding Density Matrix Renormalization Group. *J. Chem. Theory Comput.* **2016**, *12*, 4242–4253.

- (52) Prager, S.; Zech, A.; Aquilante, F.; Dreuw, A.; Wesolowski, T. A. First time combination of frozen density embedding theory with the algebraic diagrammatic construction scheme for the polarization propagator of second order. *J. Chem. Phys.* **2016**, *144*, 204103.
- (53) Höfener, S.; Gomes, A. S. P.; Visscher, L. Solvatochromic shifts from coupled-cluster theory embedded in density functional theory. *J. Chem. Phys.* **2013**, *139*, 104106.
- (54) Macetti, G.; Genoni, A. Quantum Mechanics / Extremely Localized Molecular Orbital Embedding Strategy for Excited-States. 1. Coupling to Time-Dependent Density Functional Theory. **2020**,
- (55) Macetti, G.; Genoni, A. Quantum Mechanics / Extremely Localized Molecular Orbital Embedding Strategy for Excited-States. 2. Coupling to the Equation-of-Motion Coupled Cluster Method. **2020**,
- (56) Daday, C.; König, C.; Valsson, O.; Neugebauer, J.; Filippi, C. State-Specific Embedding Potentials for Excitation-Energy Calculations. *J. Chem. Theory Comput.* **2013**, *9*, 2355–2367.
- (57) Daday, C.; König, C.; Neugebauer, J.; Filippi, C. Wavefunction in Density Functional Theory Embedding for Excited States: Which Wavefunctions, which Densities? *Chem. Phys. Chem.* **2014**, *15*, 3205–3217.
- (58) Dresselhaus, T.; Neugebauer, J.; Knecht, S.; Keller, S.; Ma, Y.; Reiher, M. Self-consistent embedding of density-matrix renormalization group wavefunctions in a density functional environment. *J. Chem. Phys.* **2015**, *142*, 044111.
- (59) Höfener, S.; Visscher, L. Wave Function Frozen-Density Embedding: Coupled Excitations. *J. Chem. Theory Comput.* **2016**, *12*, 549–557.

- (60) de Lima Batista, A. P.; de Oliveira-Filho, A. G. S.; Galembeck, S. E. Photophysical properties and the NO photorelease mechanism of a ruthenium nitrosyl model complex investigated using the CASSCF-in-DFT embedding approach. *Phys. Chem. Chem. Phys.* **2017**, *19*, 13860–13867.
- (61) Wen, X.; Graham, D. S.; Chulhai, D. V.; Goodpaster, J. D. Absolutely Localized Projection-Based Embedding for Excited States. *J. Chem. Theory Comput.* **2020**, *16*, 385–398.
- (62) Geertsen, J.; Rittby, M.; Bartlett, R. J. The equation-of-motion coupled-cluster method: Excitation energies of Be and CO. *Chem. Phys. Lett.* **1989**, *164*, 57 – 62.
- (63) Watts, J. D. In *Radiation Induced Molecular Phenomena in Nucleic Acids: A Comprehensive Theoretical and Experimental Analysis*; Shukla, M. K., Leszczynski, J., Eds.; Springer Netherlands: Dordrecht, 2008; pp 65–92.
- (64) Ding, F.; Tsuchiya, T.; Manby, F. R.; Miller, T. F. Linear-Response Time-Dependent Embedded Mean-Field Theory. *J. Chem. Theory Comput.* **2017**, *13*, 4216–4227.
- (65) Knizia, G.; Chan, G. K.-L. Density Matrix Embedding: A Simple Alternative to Dynamical Mean-Field Theory. *Phys. Rev. Lett.* **2012**, *109*, 186404.
- (66) Knizia, G.; Chan, G. K.-L. Density Matrix Embedding: A Strong-Coupling Quantum Embedding Theory. *J. Chem. Theory Comput.* **2013**, *9*, 1428–1432.
- (67) Welborn, M.; Tsuchimochi, T.; Van Voorhis, T. Bootstrap embedding: An internally consistent fragment-based method. *J. Chem. Phys.* **2016**, *145*, 074102.
- (68) Ye, H.-Z.; Welborn, M.; Ricke, N. D.; Van Voorhis, T. Incremental embedding: A density matrix embedding scheme for molecules. *J. Chem. Phys.* **2018**, *149*, 194108.
- (69) Hermes, M. R.; Gagliardi, L. Multiconfigurational Self-Consistent Field Theory with

- Density Matrix Embedding: The Localized Active Space Self-Consistent Field Method. *J. Chem. Theory Comput.* **2019**, *15*, 972–986.
- (70) Pham, H. Q.; Bernales, V.; Gagliardi, L. Can Density Matrix Embedding Theory with the Complete Activate Space Self-Consistent Field Solver Describe Single and Double Bond Breaking in Molecular Systems? *J. Chem. Theory Comput.* **2018**, *14*, 1960–1968.
- (71) Lan, T. N.; Zgid, D. Generalized Self-Energy Embedding Theory. *J. Phys. Chem. Lett.* **2017**, *8*, 2200–2205.
- (72) Mi, W.; Pavanello, M. Nonlocal Subsystem Density Functional Theory. *J. Phys. Chem. Lett.* **2020**, *11*, 272–279.
- (73) Tran, H. K.; Van Voorhis, T.; Thom, A. J. W. Using SCF meta-dynamics to extend density matrix embedding theory to excited states. *J. Chem. Phys.* **2019**, *151*.
- (74) Cui, Z.-H.; Zhu, T.; Chan, G. K.-L. Efficient Implementation of *Ab Initio* Quantum Embedding in Periodic Systems: Density Matrix Embedding Theory. *J. Chem. Theory Comput.* **2020**, *16*, 119–129.
- (75) Ricke, N.; Welborn, M.; Ye, H.-Z.; Van Voorhis, T. Performance of Bootstrap Embedding for long-range interactions and 2D systems. *Mol. Phys.* **2017**, *115*, 2242–2253.
- (76) Ye, H.-Z.; Ricke, N. D.; Tran, H. K.; Van Voorhis, T. Bootstrap Embedding for Molecules. *J. Chem. Theory Comput.* **2019**, *15*, 4497–4506.
- (77) Ye, H.-Z.; Van Voorhis, T. Atom-Based Bootstrap Embedding For Molecules. *J. Phys. Chem. Lett.* **2019**, *10*, 6368–6374.
- (78) Ye, H.-Z.; Tran, H. K.; Van Voorhis, T. Bootstrap Embedding For Large Molecular Systems. *J. Chem. Theory Comput.* **2020**, *16*, 5035–5046.

- (79) Tran, H. K.; Ye, H.-Z.; Van Voorhis, T. Bootstrap embedding with an unrestricted mean-field bath. *J. Chem. Phys.* **2020**, *153*, 0000.
- (80) Møller, C.; Plesset, M. S. Note on an Approximation Treatment for Many-Electron Systems. *Phys. Rev.* **1934**, *46*, 618–622.
- (81) III, G. D. P.; Bartlett, R. J. A full coupled-cluster singles and doubles model: The inclusion of disconnected triples. *J. Chem. Phys.* **1982**, *76*, 1910–1918.
- (82) Ahlrichs, R.; Scharf, P. In *Advances in Chemical Physics: Ab Initio Methods in Quantum Chemistry*; Lawley, K. P., Ed.; John Wiley & Sons, Inc.: Hoboken, NJ, USA, 1987; Vol. 67.
- (83) Ye, H.-Z.; Welborn, M.; Ricke, N. D.; Van Voorhis, T. σ -SCF: A direct energy-targeting method to mean-field excited states. *J. Chem. Phys.* **2017**, *147*, 214104.
- (84) Ye, H.-Z.; Van Voorhis, T. Half-Projected σ Self-Consistent Field For Electronic Excited States. *J. Chem. Theory Comput.* **2019**, *15*, 2954–2965.
- (85) Zhao, L.; Neuscamman, E. An Efficient Variational Principle for the Direct Optimization of Excited States. *J. Chem. Theory Comput.* **2016**, *12*, 3436–3440.
- (86) Shea, J. A. R.; Neuscamman, E. Communication: A mean field platform for excited state quantum chemistry. *J. Chem. Phys.* **2018**, *149*, 081101.
- (87) Shea, J. A. R.; Gwin, E.; Neuscamman, E. A Generalized Variational Principle with Applications to Excited State Mean Field Theory. *J. Chem. Theory Comput.* **2020**, *16*, 1526–1540.
- (88) Zhao, L.; Neuscamman, E. Density Functional Extension to Excited-State Mean-Field Theory. *J. Chem. Theory Comput.* **2020**, *16*, 164–178.
- (89) Hait, D.; Head-Gordon, M. Excited State Orbital Optimization via Minimizing the Square of the Gradient: General Approach and Application to Singly and Doubly

- Excited States via Density Functional Theory. *J. Chem. Theory Comput.* **2020**, *16*, 1699–1710.
- (90) Hait, D.; Head-Gordon, M. Highly Accurate Prediction of Core Spectra of Molecules at Density Functional Theory Cost: Attaining Sub-electronvolt Error from a Restricted Open-Shell Kohn-Sham Approach. *J. Chem. Theory Comput.* **2020**, *11*, 775–786.
- (91) Carter-Fenk, K.; Herbert, J. M. State-Targeted Energy Projection: A Simple and Robust Approach to Orbital Relaxation of Non-Aufbau Self-Consistent Field Solutions. *J. Chem. Theory Comput.* **2020**, *16*, 5067–5082.
- (92) Tran, L. N.; Shea, J. A. R.; Neuscamman, E. Tracking Excited States in Wave Function Optimization Using Density Matrices and Variational Principles. *J. Chem. Theory Comput.* **2019**, *15*, 4790–4803.
- (93) Kowalczyk, T.; Tsuchimochi, T.; Chen, P.-T.; Top, L.; Van Voorhis, T. Excitation energies and Stokes shifts from a restricted open-shell Kohn-Sham approach. *J. Chem. Phys.* **2013**, *138*, 164101.
- (94) Hellman, A.; Razaznejad, B.; Lundqvist, B. I. Potential-energy surfaces for excited states in extended systems. *J. Chem. Phys.* **2004**, *120*, 4593 – 4602.
- (95) Gavnholt, J.; Olsen, T.; Englund, M.; Schiøtz, J. Δ self-consistent field method to obtain potential energy surfaces of excited molecules on surfaces. *Phys. Rev. B* **2008**, *78*, 075441.
- (96) Szabo, A.; Ostlund, N. S. *Modern Quantum Chemistry: Introduction to Advanced Electronic Structure Theory*; Dover Publications Inc.: Mineola, New York, 1996.
- (97) Hohenberg, P.; Kohn, W. Inhomogeneous Electron Gas. *Phys. Rev.* **1964**, *136*, B864–B871.

- (98) Kohn, W.; Sham, L. J. Self-Consistent Equations Including Exchange and Correlation Effects. *Phys. Rev.* **1965**, *140*, A1133–A1138.
- (99) Dreuw, A.; Head-Gordon, M. Single-Reference *ab initio* Methods for the Calculation of Excited States of Large Molecules. *Chem. Rev.* **2005**, *105*, 4009–4037.
- (100) Hirata, S.; Fan, P.-D.; Shiozaki, T.; Shigeta, Y. In *Radiation Induced Molecular Phenomena in Nucleic Acids: A Comprehensive Theoretical and Experimental Analysis*; Shukla, M. K., Leszczynski, J., Eds.; Springer Netherlands: Dordrecht, 2008; pp 15–64.
- (101) Dreuw, A.; Head-Gordon, M. Failure of Time-Dependent Density Functional Theory for Long-Range Charge-Transfer Excited States: The Zincbacteriochlorin-Bacteriochlorin and Bacteriochlorophyll-Spheroidene Complexes. **2004**, *126*, 4007 – 4016.
- (102) Cheng, C.-L.; Wu, Q.; Van Voorhis, T. Rydberg energies using excited state density functional theory. *J. Chem. Phys.* **2008**, *129*, 124112.
- (103) Ziegler, T.; Krykunov, M. On the calculation of charge transfer transitions with standard density functionals using constrained variational density functional theory. *J. Chem. Phys.* **2010**, *133*, 074104.
- (104) Elliott, P.; Goldson, S.; Canahui, C.; Maitra, N. T. Perspectives on double-excitations in TDDFT. *Chem. Phys.* **2011**, *391*, 110 – 119.
- (105) Ye, H.-Z.; Van Voorhis, T. Self-consistent Møller-Plesset Perturbation Theory For Excited States. 2020.
- (106) Lee, J.; Small, D. W.; Head-Gordon, M. Excited states via coupled cluster theory without equation-of-motion methods: Seeking higher roots with application to doubly excited states and double core hole states. *J. Chem. Phys.* **2019**, *151*, 214103.

- (107) Gilbert, A. T. B.; Besley, N. A.; Gill, P. M. W. Self-Consistent Field Calculations of Excited States Using the Maximum Overlap Method (MOM). *2008*, *112*, 13164 – 13171.
- (108) Bulik, I. W.; Scuseria, G. E.; Dukelsky, J. Density matrix embedding from broken symmetry lattice mean fields. *Phys. Rev. B* **2014**, *89*, 035140.
- (109) Ekert, A.; Knight, P. L. Entangled quantum systems and the Schmidt decomposition. *Am. J. Phys.* **1995**, *63*, 415–423.
- (110) Klich, I. Lower entropy bounds and particle number fluctuations in a Fermi sea. *J. Phys. A: Math. Gen.* **2006**, *39*, L85.
- (111) Peschel, I.; Eisler, V. Reduced density matrices and entanglement entropy in free lattice models. *J. Phys. A: Math. Theor.* **2009**, *42*, 504003.
- (112) Peschel, I. Special Review: Entanglement in Solvable Many-Particle Models. *Braz. J. Phys.* **2012**, *42*, 267–291.
- (113) Knizia, G. Intrinsic Atomic Orbitals: An Unbiased Bridge between Quantum Theory and Chemical Concepts. *J. Chem. Theory Comput.* **2013**, *9*, 4834–4843.
- (114) Boys, S. F. Construction of Some Molecular Orbitals to Be Approximately Invariant for Changes from One Molecule to Another. *Rev. Mod. Phys.* **1960**, *32*, 296–299.
- (115) Wouters, S.; Jiménez-Hoyos, C. A.; Sun, Q.; Chan, G. K.-L. A Practical Guide to Density Matrix Embedding Theory in Quantum Chemistry. *J. Chem. Theory Comput.* **2016**, *12*, 2706–2719, PMID: 27159268.
- (116) Lau, B. T. G.; Knizia, G.; Berkelbach, T. C. Regional Embedding Enables High-Level Quantum Chemistry for Surface Science. *J. Phys. Chem. Lett.* **2021**, *12*, 1104–1109.
- (117) G. Knizia, unpublished.

- (118) Becke, A. D. A new mixing of Hartree-Fock and local density-functional theories. *J. Chem. Phys.* **1993**, *98*, 1372–1377.
- (119) Ditchfield, R.; Hehre, W. J.; Pople, J. A. Self-Consistent Molecular-Orbital Methods. IX. An Extended Gaussian-Type Basis for Molecular-Orbital Studies of Organic Molecules. *J. Chem. Phys.* **1971**, *54*.
- (120) Hehre, W. J.; Ditchfield, R.; Pople, J. A. Self-Consistent Molecular Orbital Methods. XII. Further Extensions of Gaussian-Type Basis Sets for Use in Molecular Orbital Studies of Organic Molecules. *J. Chem. Phys.* **1972**, *56*.
- (121) Hariharan, P. C.; Pople, J. A. The influence of polarization functions on molecular orbital hydrogenation energies. *Theor. Chim. Acta* **1973**, *28*.
- (122) Gordon, M. S.; Binkley, J. S.; Pople, J. A.; Pietro, W. J.; Hehre, W. J. Self-consistent molecular-orbital methods. 22. Small split-valence basis sets for second-row elements. **1982**, *104*.
- (123) Francl, M. M.; Pietro, W. J.; Hehre, W. J.; Binkley, J. S.; Gordon, M. S.; DeFrees, D. J.; Pople, J. A. Self-consistent molecular orbital methods. XXIII. A polarization-type basis set for second-row elements. *J. Chem. Phys.* **1982**, *77*.
- (124) Shao, Y.; Gan, Z.; Epifanovsky, E.; Gilbert, A. T.; Wormit, M.; Kussmann, J.; Lange, A. W.; Behn, A.; Deng, J.; Feng, X.; Ghosh, D.; Goldey, M.; Horn, P. R.; Jacobson, L. D.; Kaliman, I.; Khaliullin, R. Z.; Kuš, T.; Landau, A.; Liu, J.; Proynov, E. I.; Rhee, Y. M.; Richard, R. M.; Rohrdanz, M. A.; Steele, R. P.; Sundstrom, E. J.; III, H. L. W.; Zimmerman, P. M.; Zuev, D.; Albrecht, B.; Alguire, E.; Austin, B.; Beran, G. J. O.; Bernard, Y. A.; Berquist, E.; Brandhorst, K.; Bravaya, K. B.; Brown, S. T.; Casanova, D.; Chang, C.-M.; Chen, Y.; Chien, S. H.; Closser, K. D.; Crittenden, D. L.; Diedenhofen, M.; Jr., R. A. D.; Do, H.; Dutoi, A. D.; Edgar, R. G.; Fatehi, S.;

- Fusti-Molnar, L.; Ghysels, A.; Golubeva-Zadorozhnaya, A.; Gomes, J.; Hanson-Heine, M. W.; Harbach, P. H.; Hauser, A. W.; Hohenstein, E. G.; Holden, Z. C.; Jagau, T.-C.; Ji, H.; Kaduk, B.; Khistyayev, K.; Kim, J.; Kim, J.; King, R. A.; Klunzinger, P.; Kosenkov, D.; Kowalczyk, T.; Krauter, C. M.; Lao, K. U.; Laurent, A. D.; Lawler, K. V.; Levchenko, S. V.; Lin, C. Y.; Liu, F.; Livshits, E.; Lochan, R. C.; Lusenier, A.; Manohar, P.; Manzer, S. F.; Mao, S.-P.; Mardirossian, N.; Marenich, A. V.; Maurer, S. A.; Mayhall, N. J.; Neuscamman, E.; Oana, C. M.; Olivares-Amaya, R.; O'Neill, D. P.; Parkhill, J. A.; Perrine, T. M.; Peverati, R.; Prociuk, A.; Rehn, D. R.; Rosta, E.; Russ, N. J.; Sharada, S. M.; Sharma, S.; Small, D. W.; Sodt, A.; Stein, T.; Stück, D.; Su, Y.-C.; Thom, A. J.; Tsuchimochi, T.; Vanovschi, V.; Vogt, L.; Vydrov, O.; Wang, T.; Watson, M. A.; Wenzel, J.; White, A.; Williams, C. F.; Yang, J.; Yeganeh, S.; Yost, S. R.; You, Z.-Q.; Zhang, I. Y.; Zhang, X.; Zhao, Y.; Brooks, B. R.; Chan, G. K.; Chipman, D. M.; Cramer, C. J.; III, W. A. G.; Gordon, M. S.; Hehre, W. J.; Klamt, A.; III, H. F. S.; Schmidt, M. W.; Sherrill, C. D.; Truhlar, D. G.; Warshel, A.; Xu, X.; Aspuru-Guzik, A.; Baer, R.; Bell, A. T.; Besley, N. A.; Chai, J.-D.; Dreuw, A.; Dunietz, B. D.; Furlani, T. R.; Gwaltney, S. R.; Hsu, C.-P.; Jung, Y.; Kong, J.; Lambrecht, D. S.; Liang, W.; Ochsenfeld, C.; Rassolov, V. A.; Slipchenko, L. V.; Subotnik, J. E.; Van Voorhis, T.; Herbert, J. M.; Krylov, A. I.; Gill, P. M.; Head-Gordon, M. Advances in molecular quantum chemistry contained in the Q-Chem 4 program package. *Mol. Phys.* **2015**, *113*, 184–215.
- (125) Sun, Q.; Berkelbach, T. C.; Blunt, N. S.; Booth, G. H.; Guo, S.; Li, Z.; Liu, J.; McClain, J. D.; Sayfutyarova, E. R.; Sharma, S.; Wouters, S.; Chan, G. K. PySCF: the Python-based simulations of chemistry framework. 2017.
- (126) Valeev, E. F. Libint: A library for the evaluation of molecular integrals of many-body operators over Gaussian functions. <http://libint.valeyev.net>, 2018.
- (127) Eichkorn, K.; Treutler, O.; Öhm, H.; Häser, M.; Ahlrichs, R. Auxiliary basis sets to

- approximate Coulomb potentials. *Chem. Phys. Lett.* **1995**, *240*, 283 – 290.
- (128) Eichkorn, K.; Weigend, F.; Treutler, O.; Ahlrichs, R. Auxiliary basis sets for main row atoms and transition metals and their use to approximate Coulomb potentials. *Theor. Chim. Acta* **1997**, *97*, 119–124.
- (129) Weigend, F. Accurate Coulomb-fitting basis sets for H to Rn. *Phys. Chem. Chem. Phys.* **2006**, *8*, 1057–1065.
- (130) Weigend, F. A fully direct RI-HF algorithm: Implementation, optimised auxiliary basis sets, demonstration of accuracy and efficiency. *Phys. Chem. Chem. Phys.* **2002**, *4*, 4285–4291.
- (131) Whitten, J. L. Coulombic potential energy integrals and approximations. *J. Chem. Phys.* **1973**, *58*, 4496–4501.
- (132) Häser, M.; Ahlrichs, R. Improvements on the direct SCF method. *J. Comput. Chem.* **1989**, *10*, 104–111.
- (133) Strout, D. L.; Scuseria, G. E. A quantitative study of the scaling properties of the Hartree-Fock method. *J. Chem. Phys.* **1995**, *102*, 8448–8452.
- (134) Lambrecht, D. S.; Doser, B.; Ochsenfeld, C. Rigorous integral screening for electron correlation methods. *J. Chem. Phys.* **2005**, *123*, 184102.
- (135) Dunning, T. H. Gaussian basis sets for use in correlated molecular calculations. I. The atoms boron through neon and hydrogen. *J. Chem. Phys.* **1989**, *90*.
- (136) Woon, D. E.; Dunning, T. H. Gaussian basis sets for use in correlated molecular calculations. III. The atoms aluminum through argon. *J. Chem. Phys.* **1993**, *98*.
- (137) Weigend, F.; Köhn, A.; Hättig, C. Efficient use of the correlation consistent basis sets in resolution of the identity MP2 calculations. *J. Chem. Phys.* **2002**, *116*.

- (138) Weigend, F.; Ahlrichs, R. Balanced basis sets of split valence, triple zeta valence and quadruple zeta valence quality for H to Rn: Design and assessment of accuracy. *Phys. Chem. Chem. Phys.* **2005**, *7*.
- (139) Weigend, F.; Häser, M.; Patzelt, H.; Ahlrichs, R. RI-MP2: optimized auxiliary basis sets and demonstration of efficiency. *Chem. Phys. Lett.* **1998**, *294*.
- (140) Sun, J. W.; Kim, K.-H.; Moon, C.-K.; Lee, J.-H.; Kim, J.-J. Highly Efficient Sky-Blue Fluorescent Organic Light Emitting Diode Based on Mixed Cohost System for Thermally Activated Delayed Fluorescence Emitter (2CzPN). *ACS Appl. Mater. Interfaces* **2016**, *8*, 9806–9810.
- (141) Cotts, B. L.; McCarthy, D. G.; Noriega, R.; Penwell, S. B.; Delor, M.; Devore, D. D.; Mukhopadhyay, S.; De Vries, T. S.; Ginsberg, N. S. Tuning Thermally Activated Delayed Fluorescence Emitter Photophysics through Solvation in the Solid State. *ACS Energy Lett.* **2017**, *2*, 1526–1533.
- (142) Penfold, T. J.; Dias, F. B.; Monkman, A. P. The theory of thermally activated delayed fluorescence for organic light emitting diodes. *Chem. Commun.* **2018**, *54*, 3926–3935.
- (143) Greenspan, P.; Mayer, E. P.; Fowler, S. D. Nile red: a selective fluorescent stain for intracellular lipid droplets. *J. Cell Biol.* **1985**, *100*, 965–973.
- (144) Schlegel, H. B. Potential energy curves using unrestricted Møller-Plesset perturbation theory with spin annihilation. *J. Chem. Phys.* **1986**, *84*, 4530–4534.
- (145) Gill, P. M. W.; Pople, J. A.; Radom, L.; Nobes, R. H. Why does unrestricted Møller-Plesset perturbation theory converge so slowly for spin-contaminated wave functions? *J. Chem. Phys.* **1988**, *89*, 7307–7314.
- (146) Kurlancheek, W.; Head-Gordon, M. Violations of N -representability from spin-

- unrestricted orbitals in Møller-Plesset perturbation theory and related double-hybrid density functional theory. **2009**, *107*, 1223–1232.
- (147) Rettig, A.; Hait, D.; Bertels, L. W.; Head-Gordon, M. Third-Order Møller-Plesset Theory Made More Useful? The Role of Density Functional Theory Orbitals. *J. Chem. Theory Comput.* **2020**, *0*, 0000.
- (148) Pitoňák, M.; Neogrady, P.; Černý, J.; Grimme, S.; Hobza, P. Scaled MP3 Non-Covalent Interaction Energies Agree Closely with Accurate CCSD(T) Benchmark Data. *Chem. Phys. Chem.* **2009**, *10*, 282–289.
- (149) Riley, K. E.; Řezáč, J.; Hobza, P. The performance of MP2.5 and MP2.X methods for nonequilibrium geometries of molecular complexes. *Phys. Chem. Chem. Phys.* **2012**, *14*, 13187–13193.
- (150) Sedlak, R.; Riley, K. E.; Řezáč, J.; Pitoňák, M.; Hobza, P. MP2.5 and MP2.X: Approaching CCSD(T) Quality Description of Noncovalent Interaction at the Cost of a Single CCSD Iteration. *Chem. Phys. Chem.* **2013**, *14*, 698–707.
- (151) Bozkaya, U.; Sherrill, C. D. Orbital-optimized MP2.5 and its analytic gradients: Approaching CCSD(T) quality for noncovalent interactions. *J. Chem. Phys.* **2014**, *141*, 204105.
- (152) Bertels, L. W.; Lee, J.; Head-Gordon, M. Third-Order Møller-Plesset Perturbation Theory Made Useful? Choice of Orbitals and Scaling Greatly Improves Accuracy for Thermochemistry, Kinetics, and Intermolecular Interactions. *J. Phys. Chem. Lett.* **2019**, *10*, 4170–4176.
- (153) Bulik, I. W.; Chen, W.; Scuseria, G. E. Electron correlation in solids via density embedding theory. *J. Chem. Phys.* **2014**, *141*, 054113.